# A Battery-Free Tag for Wireless Monitoring of Heart Sounds

Soumyajit Mandal, Lorenzo Turicchia, Rahul Sarpeshkar
Dept. of Electrical Engineering & Computer Science
Massachusetts Institute of Technology
Cambridge, MA 02139
Email: rahuls@mit.edu

***Abstract*—We have developed a wearable, battery-free tag that monitors heart sounds. The tag powers up by harvesting ambient RF energy, and contains a low-power integrated circuit, an antenna and up to four microphones. The chip, which consumes only 1.0$\mu$W of power, generates digital events when the outputs of any of the microphones exceeds a programmable threshold voltage, combines such events together by using a programmable logic array, and transmits them to a base station by using backscatter modulation. The chip can also be programmed to trade-off microphone sensitivity for power consumption. In this paper, we demonstrate that the tag, when attached to the chest, can reliably measure heart rate at distances up to 7m from an FCC-compliant RF power source. We also suggest how delays between signals measured by microphones at the wrist and neck can be used to provide information about relative blood-pressure variations.**

## I. Introduction

Mechanical coupling causes the skin to vibrate in synchrony with motions of the heart. Such vibrations generate acoustic pressure waves, referred to as heart sounds, that can be picked by microphones or by trained human ears using stethoscopes. Such sounds provide important information about cardiac health. For example, consider the characteristic *lub/dub* rhythm present within each heart beat, referred to as the first heart sound ($S_1$) and second heart sound ($S_2$), respectively. These sounds are produced by the turbulent flow of blood against the closed atrioventricular and semilunar valves, respectively, and are thus sensitive to the condition of these valves. The resting value and short-term variability of the heart rate, which are both of clinical importance [1], can also be measured from such acoustical recordings, known as phono-cardiograms (PCGs).

Continuous monitoring and analysis of heart sounds is likely to provide important health benefits because these sounds contain large amounts of useful information. Most obviously, the cessation of a regular heart beat can be used to detect Sudden Cardiac Arrest (SCA). More than 5,000 people experience SCA every week in the United States alone. The only definitive treatment for SCA is early defibrillation: no more than 6 minutes from arrest to first shock. The chance for survival drops 10% per minute without defibrillation, and today, over 95% of SCA victims die. Since automatic defibrillators are increasingly available, continuous monitoring of those at risk can save many lives [2]. In addition, cardiac arrhythmias, some of which can be life-threatening, can be detected from heart-rate data. In the United States alone, approximately 2,000 infants die each year from Sudden Infant Death Syndrome (SIDS). Since slow heart rate (bradycardia) is an important indicator of SIDS [3], early detection of bradycardia in infants may save many lives each year.

In this paper, we describe a low-cost wearable tag that can be attached to the skin and used for continuous wireless monitoring of heart sounds. In order to be effective, such monitoring systems should be widely adopted, which means that they must be unobtrusive, robust, and low-cost. One way to lower the size, weight and cost of the system is to eliminate batteries and rely entirely on harvested ambient energy, in this case RF. This is the approach adopted by passive radio-frequency identification (RFID) tags [4], which face similar size and cost constraints. However, maintaining reliable and robust operation is challenging for any biomedical device, but particularly problematic when a reliable local energy source, such as a battery, is absent. We describe algorithms that detect malfunctioning tags, thereby improving the reliability of our results.

In this paper, we have chosen to focus on sounds, not electrical signals, for monitoring heart activity. There are two main advantages of this approach. Firstly, listening to heart sounds does not require any electrical contact to be established with the body. Such contacts are particularly difficult to establish when the skin is dry. As a result, long-term acoustical recordings can be obtained with less regular maintenance than comparable electrical recordings, such as the electro-cardiogram or EKG. Secondly, the heart is easy to sense acoustically as it is the loudest organ in the body. As a result heart sounds can be monitored in a very low-power fashion with a cheap microphone. Reducing power consumption becomes extremely important for systems such as ours that rely on energy-harvesting, since the available ambient energy density is usually orders of magnitude lower than that present within a battery.

## II. System Design

A conceptual view of our tag and a photograph of the prototype that was actually tested are shown in Figure 1. We estimate that the area of the prototype, which contains the chip, an antenna for RF energy harvesting, and two microphones,

978-0-7695-3644-6/09 $25.00 © 2009 IEEE
DOI 10.1109/BSN.2009.11

can easily be halved by using a smaller package for the chip and a more optimized antenna. The two microphones are used to generate three types of alarm: disconnection from the body, device malfunction, and patient emergency. One microphone faces up (away from the body) and the other faces down. The downward-facing microphone monitors heart sounds, while the upward-facing one is usually switched off to save power. It is turned on only when the downward-facing microphone does not detect any heart sounds and a disconnection or patient emergency is suspected. If both microphones now pick up similar environmental sounds, a 'disconnection alarm' is generated since it is probable that the tag is no longer in proximity to the skin. A 'patient emergency alarm' is generated if the downward-facing microphone does not pick up environmental sounds, but the upward-facing one does, since in this case it is likely that the tag is still attached and the heart has stopped. If neither microphone picks up any sounds, the tag is probably malfunctioning; therefore a 'device malfunction alarm' is generated.

Each tag contains a unique identification code. A fixed base station communicates with multiple tags and decides if and when an alarm should be triggered. Tags that were earlier actively communicating with the base station, but have since stopped doing so, may have left the area covered by the base station, or entered an area with insufficient RF energy for reliable operation. Software on the base station must be able to distinguish between such events and alarms generated by disconnections, patient emergencies and tag malfunctions.

Our tag is battery-less and operates by harvesting radiated RF energy [5], [6]. We now calculate the available power $P_A$ that can be harvested at different distances $D$ from the RF transmitter. Path loss models predict the fall-off of radiated power density $P_r$ (in W/m$^2$) with $D$. A simple version commonly used for modeling indoor environments recognizes two propagation zones: $P_r \propto D^{-n_1}$ for $D \leq D_0$, and $P_r \propto D^{-n_2}$ for $D > D_0$, where $D_0$, $n_1$ and $n_2$ are constants [7]. Typically $n_1 \approx 2$, the free-space value, and $n_2$ varies between 2.5 and 4. The value of $n_2$ exceeds 2 because of absorption and reflection of the RF by environmental obstacles, such as furniture and people. Using conservative values ($D_0 = 5$m, $n_1 = 2$, $n_2 = 3.5$) and combining the predicted path loss with the rectifier model proposed in [6] gives us Figure 2. The figure assumes that the equivalent isotropic radiated power (EIRP) is 4W, which is the maximum allowed in the United States for radio-frequency identification (RFID) applications. It shows $P_A$ as a function of $D$ at two popular RFID frequencies: 900MHz and 2.4GHz. The main reason for going to higher operating frequencies is to reduce the physical size of the antenna.

The various curves in Figure 2 correspond to different load resistances $R_L$ driven by the on-chip rectifier. They decrease rapidly at large distances because the received RF amplitude becomes smaller than the rectifier's dead zone. The load resistance is usually dominated by the power consumed by off-chip sensors and not the chip itself. For example, a microphone biased at 30$\mu$A and 0.5V (typical values used

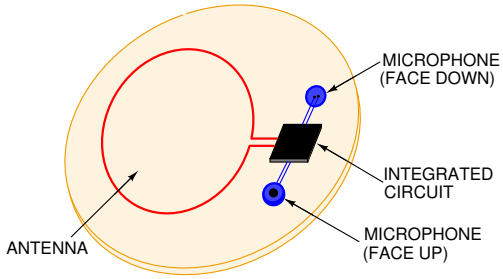


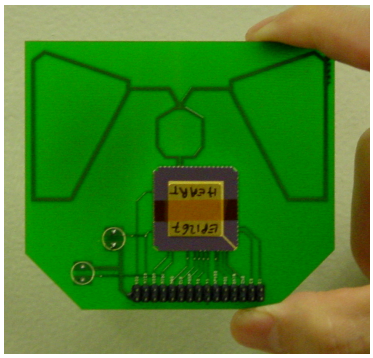

Fig. 1. Conceptual view of our tag, attached to a flexible, adhesive surface (top), and photograph of the actual 800MHz prototype that was tested experimentally (bottom). The pins at the bottom of the prototype were for testing purposes and will be removed in the final version.

in our experiments) dissipates 15$\mu$W, corresponding to an effective load driven by the rectifier of $R_L = 16.7$k$\Omega$ [6]. Figure 2 then predicts an operating range of approximately 12m at 900MHz and 3m at 2.4GHz. In practice the reliable operating range will be somewhat smaller because some tags will be mistuned by their proximity to conductive and dielectric surfaces. In addition, we have to allow for transient drops in received RF power level (fades), which are ubiquitous in indoor environments because the received signal is the superposition of multiple waves with time-varying amplitude and phase. Nevertheless, a single base-station operating at 900MHz is sufficient for a moderately-sized room.

Our chip contains four independent channels that can be used to interface to sensors such as microphones. The outputs of these channels are thresholded, or digital signals. These signals can be combined in a flexible way using a Programmable Logic Array (PLA) that can implement a variety of Boolean logic functions. Our PLA is a four-input four-output design with a $8 \times 8$ AND plane and a $4 \times 8$ OR plane. The PLA allows us to implement any of the $2^{2^4}$ possible logic functions of four inputs for any of its four outputs in a programmable fashion. These outputs can be monitored individually, allowing us to implement rudimentary sensor-fusion algorithms that combine the outputs of multiple channels. Programmable output selection logic multiplexes the four PLA outputs into

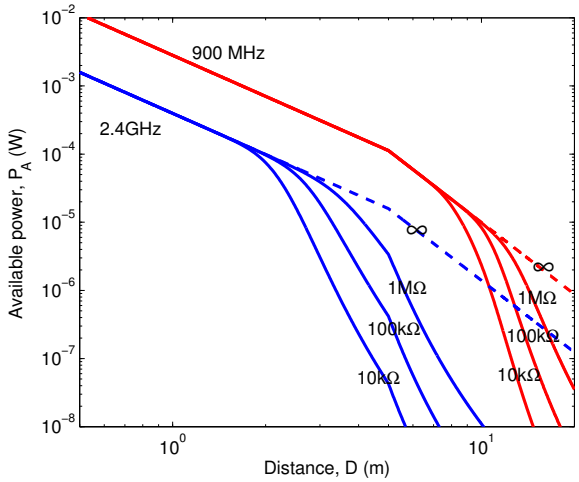


Fig. 2. Theoretical limits on harvested RF power as a function of distance from the transmitter for different load resistances at 900MHz and 2.4GHz.

a single signal that is transmitted to the base station as "event packets" containing the chip identification code and time stamps. Data is transmitted using backscatter modulation [4]: a 100fF capacitor is added and subtracted from $C_L$ to change the amount of RF power scattered by the tag. Backscatter modulation is popular in passive RFID systems because all the complexity and power consumption is pushed to the base station; the tag remains simple and low-power.

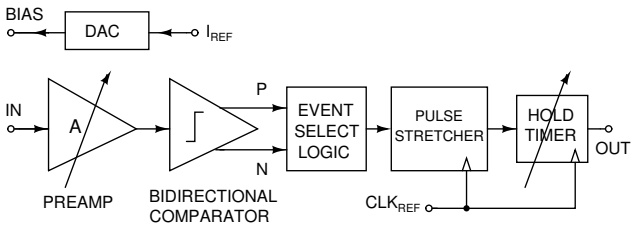


Fig. 3. A single on-chip signal-processing channel.

A block diagram of a single channel is shown in Figure 3. The preamplifier consists of a common source stage with capacitive feedback. The size of the feedback capacitor can be varied between $C_0$ and $16C_0$ to set the gain. The amplifier incorporates DC rejection, i.e., the transfer function is band-pass with a very low cut-in frequency (typically $<$1Hz). It uses a nominal bias current of 10nA and $C_0 = 0.5$pF resulting in a bandwidth that decreases from 12KHz to 6KHz as the gain increases from 1 to 16. A matched copy of the amplifier (minus the capacitors) is used to determine the quiescent operating point.

The comparator generates events whenever the output voltage of the amplifier differs from its quiescent value by more than a fixed threshold voltage $V_{th} = 80$mV. There are two types of events: positive-going, when the output voltage is larger than its quiescent value by $V_{th}$ or more, and negative-going, when it is smaller. The smallest input amplitude that triggers an event decreases from $V_{th}$ to $V_{th}/16$ (80mV to 5mV) as the preamplifier gain increases from 1 to 16.

Event selection logic is connected to the comparator output in each channel and allows only positive or negative-going events, both, or neither to be detected. This combinational block is followed by a pulse-stretcher circuit that adds hysteresis in the time domain to prevent multiple comparator transitions due to noise when an event is detected. It also ensures that output events always last long enough for at least one complete data packet to be broadcast during every event. The pulse-stretcher circuit is a digitally-timed one-shot: It allows an incoming event edge to set its output high, and a delayed version of this edge to reset it low. The pulse-stretcher is followed by a programmable hold timer circuit. This circuit imposes a hold time $T_{hold}$ after each event, during which no new events can be generated. By placing an upper bound of $1/T_{hold}$ on the event rate, the hold timer greatly reduces the probability of timing collisions between different tags. The average value of $T_{hold}$ can be varied between 94ms and 1.4s.

A programmable DC current source was designed for every channel. This current source can be used to power up external sensors, such as microphones, and consists of a 8-bit binary-weighted current DAC that can supply between 0.5$\mu$A and 128$\mu$A. To reduce power consumption, the chip was designed to operate on power supply voltages as low as 0.8V (core) and 0.5V (programmable current sources).

An on-chip serial interface allows the user to program the PLA, channel selection logic, 16-bit chip identification code and channel parameters such as sensor current, preamplifier gain and hold time. The static power consumption of the chip alone is only 1.0$\mu$W. The power consumption with microphones connected is variable, since it depends on their bias currents, which can be programmed by the user.

## III. Microphone Interface

We used a microphone to detect heart sounds. Microphone responses are bandpass, with typical lower (cut-in) frequencies between 20Hz and 100Hz and upper (cut-off) frequencies between 16kHz and 20kHz. Commercial electret microphones contain built-in low-noise JFETs for buffering [8]. There are two common configurations, as shown in Figure 4. In two-terminal microphones, shown on the left, the drain of the n-type JFET, which is normally a depletion-mode device, acts as the output terminal. It is usually connected to an an external resistive load, creating a common-source amplifier. The gate voltage is internally tied to ground at DC with the large resistor $R_{big}$, while $C_{par}$ is a small, unwanted parasitic capacitance. The incoming sound pressure wave creates the voltage source $v_{elec}$ in series with the electret capacitance $C_{elec}$. Three-terminal microphones, shown on the right, configure the JFET as a source follower, and are typically more expensive.

We used a two-terminal microphone, but replaced the resistive load with a programmable current source $I_{bias}$ running off a very low supply voltage, $V_{DD,MIC}$ to save power. In this

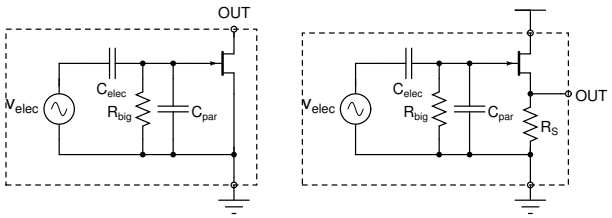


Fig. 4. Circuit diagram of common electret microphones, two-terminal (left) and three-terminal (right).

regime the JFET is unsaturated and acts as a voltage-controlled resistor. Using the standard long-channel FET equation,

$$I_{bias} = \beta \left[ V_{DSAT} V_{OUT} - V_{OUT}^2/2 \right] \quad (1)$$

where the saturation voltage $V_{DSAT}$ is fixed for a given microphone, and given approximately by $V_{GS} - V_T$, where $V_{GS}$ is the gate-to-source voltage (usually zero) and $V_T$ is the threshold voltage. Also, $V_{OUT}$ is the output voltage, and $\beta$ is a constant. Within the microphone passband the sound-generated source $v_{elec}$ changes $V_{GS}$ by an amount $v_{elec} C_{elec} / (C_{elec} + C_{par})$. Since the current through the JFET is fixed at $I_{bias}$, $v_{out}$ decreases as $v_{gs}$ increases, and vice-versa. Solving the quadratic equation in (1) and some simple small-signal analysis reveals that the transfer function between $v_{elec}$ and $v_{out}$ in the passband is

$$\frac{v_{out}}{v_{elec}} = -\frac{C_{elec}}{C_{elec} + C_{par}} \left[ \sqrt{\frac{1}{1 - I_{bias}/I_{SAT}}} - 1 \right] \quad (2)$$

where $I_{SAT} = \beta V_{DSAT}^2/2$, the JFET current in saturation, is specified by the manufacturer for a given microphone. We see that gain increases with the bias current $I_{bias}$, which we can vary by using the on-chip DAC. In reality the gain saturates at a high value as $I_{bias}$ approaches $I_{SAT}$, instead of diverging as predicted by (2), because of the finite output impedances of the saturated transistor and the current source (which we have ignored in this analysis). However, we can still trade-off sensitivity with power consumption. In fact, in this application we can save considerable amounts of power because heart sounds, which occur in the range 20-250Hz, are relatively loud and do not require large amounts of gain. We used a Panasonic omnidirectional electret condenser microphone (WM-63PR) in a plastic enclosure. The WM-63PR, which has $I_{SAT} = 500\mu$A, was selected since it is a small, thin device (diameter = 6mm, thickness = 1.3mm), has a low cut-in frequency (20Hz) and is also low-cost. Similar microphones that are even less expensive can also be used since sound quality is not important for this application.

The microphone is normally placed on the chest while monitoring heart activity. However, the membrane of the microphone cannot vibrate freely if it is located too close to the skin. Therefore we built our microphone sensor so that there is a very small cylindrical air chamber between the two. The chamber has no vents, reducing the amount of ambient noise, but its diameter and shape have little effect on sound pickup [9]. A photograph of the microphone sensor prior to mounting on the tag is shown in Figure 5.

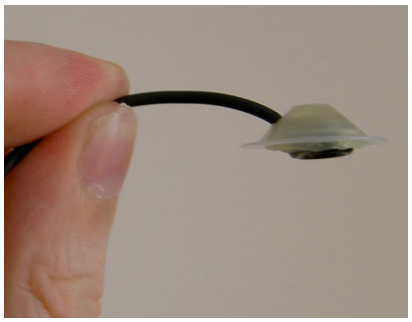

Fig. 5. Photograph of the microphone sensor used for measuring the PCG.

## IV. Experimental Results

We tested our system in a cluttered laboratory with numerous barriers to RF propagation, as shown in Figure 6. Experimentally, we were able to obtain 15$\mu$W of output power at a distance of 3.1m from an 800MHz RF source broadcasting 800mW EIRP, which was the maximum allowed by our equipment. This is enough power to run the chip and one microphone at a typical bias current of 30$\mu$A and power supply voltage of 0.5V. Increasing the transmit power to the allowed maximum of 4W should give us an operating range of 5-7m, depending upon the multipath fading characteristics of the environment. We also note that the curves in Figure 2 begin to drop off sharply with increasing distance when the received RF voltage becomes smaller than the rectifier's dead zone, which causes its power conversion efficiency to decrease rapidly. If the load resistance is such that the tag operates in this region, range can also be increased by using a smaller, but more expensive chip package with lower parasitic input capacitance $C_{in}$. Decreasing $C_{in}$ increases the quality factor of the input matching network, increasing the received RF voltage. Specifically, a given amount of available power is obtained at a distance that scales as $1/\sqrt{C_{in}}$. For example, the rectifier in [6] used a package with approximately half the input capacitance, resulting in $\sqrt{2} \approx 1.4$ times more range.

We noticed that the operation of the tag was largely unaffected by the presence of the human body up to a distance of approximately 1cm from the skin. The received power decreased sharply for smaller separations. The microphone must also be separated from the skin to operate normally. Both problems can be solved by backing the tag with dielectric foam approximately 1cm thick. Figure 7 shows measured waveforms produced by the chip in response to a single event. The backscattered signal consists of an 48-bit long event packet that is repeated for the duration of the event. Each packet begins with a 16-bit '010101...' sequence to aid synchronization, followed by the tag's unique 15-bit identification code, a parity bit and a 16-bit time-stamp. In this case three complete packets were transmitted before the event ended.

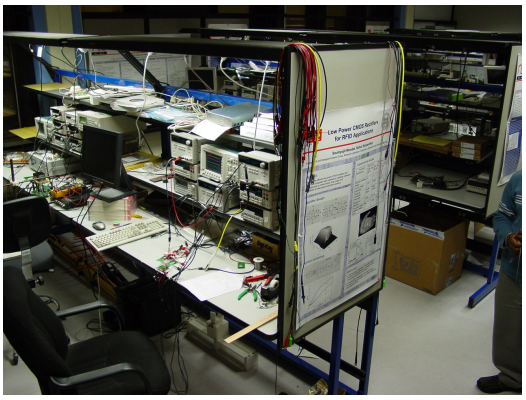

Fig. 6. Photograph of the environment within which the tag was tested.

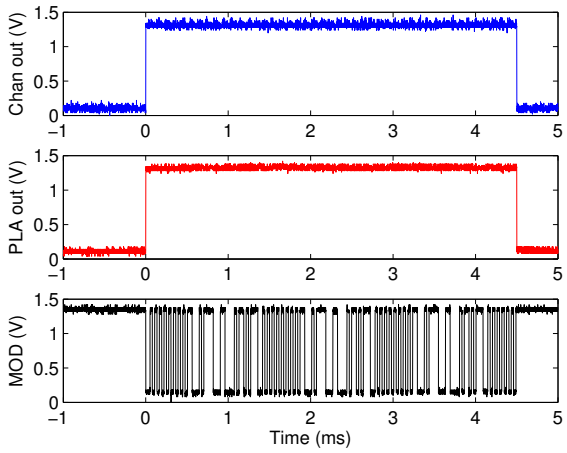


Fig. 7. Experimentally-measured waveforms generated by the chip for a single event. The figure shows (a) channel output, (b) PLA output, (c) backscattered signal.

Two tags, each containing one active microphone, were attached, respectively, to the neck and wrist of an healthy adult subject. Proximity to the carotid and radial arteries causes a strong pulse to be commonly observed at these positions. Each microphone was biased at 30$\mu$A and the preamplifier gain was set to 8. In other successful experiments (not shown) the tag was placed at its default position, the chest. In this position heart sounds are louder, enabling the microphone bias current to be further reduced.

Measured waveforms are shown in Figure 8. There are two reasons why high-frequency components, such as the $S_1$ and $S_2$ sounds found in a conventional PCG waveform, are almost completely absent in these recordings. Firstly, the coupling between the skin and the microphone is a low-pass filter. Secondly, microphone sensitivities were deliberately kept low by reducing their bias currents. This was because we were mainly interested in heart rate information, which resides in the loud, low-frequency components of the PCG (from 10 - 80Hz). Each large negative event is caused by the pulse, i.e., systolic upsurge in blood pressure and consequent dilation of the arteries. The pulse travels along arterial walls as a pressure wave, with a velocity that ranges between 5 and 15m/s but is always significantly higher than that of the blood itself. The waveform at the wrist is delayed relative to that at the neck by about 95ms because of the finite velocity of this wave, i.e., because of the time taken by the systolic pulse to propagate down the length of the arm. The delay decreases as the artery walls get stiffer or blood pressure increases, and is therefore diagnostic of atherosclerosis and hypertension [10], [11].

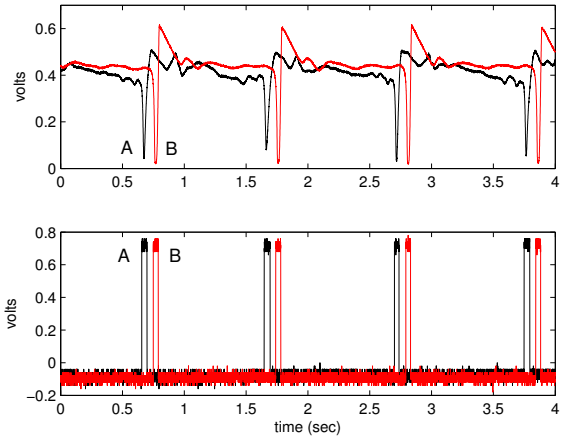


Fig. 8. Measured PCG waveforms at the neck (A) and wrist (B) of the same subject. Preamplifier (top) and channel (bottom) outputs are shown.

## V. Conclusions

We have demonstrated a programmable, low-power chip that can be powered-up by harvesting radiated RF energy. The chip forms the basis of a low-cost, battery-free tag for monitoring heart sounds, but it uses a general-purpose architecture that can be extended for wireless monitoring of other biomedical signals. Examples include the electro-cardiogram (EKG), the photo-plethysmogram (PPG) and body temperature. By enabling the pervasive monitoring of such health indicators, our chip can bring about significant improvements in the quality of life of those at risk, particularly the elderly and infants.

## References

[1] M. A. Cohen and J. A. Taylor, "Short-term cardiovascular oscillations in man: measuring and modelling the physiologies," *Journal of Physiology*, vol. 542, no. 3, pp. 669–683, 2002. [Online]. Available: http://jp.physoc.org/cgi/content/abstract/542/3/669

[2] J. J. M. de Vreede-Swagemakers, A. P. M. Gorgels, W. I. Dubois-Arbouw, J. W. van Ree, M. J. A. P. Daemen, L. G. E. Houben, and H. J. J. Wellens, "Out-of-Hospital Cardiac Arrest in the 1990s: A Population-Based Study in the Maastricht Area on Incidence, Characteristics and Survival," *Journal of the American College of Cardiology*, vol. 30, no. 6, pp. 1500–1505, Nov. 1997.

[3] R. G. Meny, J. L. Carroll, M. T. Carbone, and D. H. Kelly, "Cardiorespiratory Recordings from Infants Dying Suddenly and Unexpectedly at Home," *Pediatrics*, vol. 93, no. 1, pp. 44–49, Jan. 1994.

[4] K. Finkenzeller, *RFID Handbook: Fundamentals and Applications in Contactless Smart Cards and Identification*, 2nd ed. Chicester, Sussex, UK: John Wiley, 2003.

[5] J. R. Smith, A. P. Sample, P. S. Powledge, S. Roy, and A. Mamishev, "A Wirelessly-Powered Platform for Sensing and Computation," *Proc. Ubicomp 2006: Eighth International Conference on Ubiquitous Computing*, vol. 1, pp. 495–506, Sep. 2006.
[6] S. Mandal and R. Sarpeshkar, "Low Power CMOS Rectifier Design for RFID Applications," *IEEE Transactions on Circuits and Systems-I*, vol. 54, no. 6, pp. 1177–1188, Jun. 2007.
[7] K. S. Leong, M. L. Ng, and P. H. Cole, "Operational Considerations in Simulation and Deployment of RFID Systems," *Proc. 17th Intl. Zurich Symp. on Electromagnetic Compatibility*, vol. 1, pp. 521–524, Feb. 2006.
[8] M. W. Baker and R. Sarpeshkar, "A low-power high-PSRR current-mode microphone preamplifier," *IEEE Journal of Solid-State Circuits*, vol. 38, no. 10, pp. 1671–1678, Oct. 2003.
[9] S. S. Kraman, G. R. Wodicka, Y. Oh, and H. Pasterkamp, "Measurements of Respiratory Acoustic Signals. Effect of Microphone Air Cavity Width, Shape and Venting," *Chest*, vol. 108, no. 4, pp. 1004–1008, Oct. 1995.
[10] J. C. Bramwell and A. V. Hill, "The Velocity of the Pulse Wave in Man," *Proc. Royal Society of London. Series B*, vol. 93, no. 652, pp. 298–306, Apr. 1922.
[11] E. R. Nye, "The Effect of Blood Pressure Alteration on the Pulse Wave Velocity," *British Heart Journal*, vol. 26, no. 2, pp. 261–265, Mar. 1964.